Are Eyewall Replacement Cycles Governed Largely by Axisymmetric Balance Dynamics?

SERGIO F. ABARCA AND MICHAEL T. MONTGOMERY

Naval Postgraduate School, Monterey, California

(Manuscript received 27 May 2014, in final form 21 August 2014)

ABSTRACT

The authors question the widely held view that radial contraction of a secondary eyewall during an eyewall replacement cycle is well understood and governed largely by the classical theory of axisymmetric balance dynamics. The investigation is based on a comparison of the secondary circulation and derived tangential wind tendency between a full-physics simulation and the Sawyer–Eliassen balance model. The comparison is made at a time when the full-physics model exhibits radial contraction of the secondary eyewall during a canonical eyewall replacement cycle. It is shown that the Sawyer–Eliassen model is unable to capture the phenomenology of secondary eyewall radial contraction because it predicts a net spindown of the boundary layer tangential winds and does not represent the boundary layer spinup mechanism that has been articulated in recent work.

1. Introduction

While secondary eyewall formation (SEF) physics has been the focus of abundant contemporary research, the physics of eyewall replacement cycles (ERCs) has been widely assumed to be explained by the axisymmetric balance dynamics of convective rings [as articulated by Willoughby et al. (1982) and Shapiro and Willoughby (1982)]. This view has been explicitly and implicitly expressed in published papers (e.g., Willoughby 1988, 1990; Rozoff et al. 2008; Kepert 2010, 2013). As an example, in his insightful review paper entitled ''The dynamics of the tropical cyclone core,'' Willoughby (1988, his ''Summary'' section) described the mechanism of eyewall contraction as follows: ''Eyewalls, or other convective rings, move inward as a result of differential adiabatic heating [sic] between their inside and outside.'' In this viewpoint, the inward contraction of an eyewall is a mechanism driven by differential diabatic heating, and friction plays an unimportant role. This viewpoint continues to prevail in the current literature, as exemplified by Zhu and Zhu (2014) and by Kepert (2013, his section 6), who writes ''Once the outer RMW [radius of maximum wind] and eyewall have formed, we expect that their subsequent evolution will be governed largely by the classic theory (Shapiro and Willoughby 1982).''

Our own survey of the literature suggests that the foregoing view of eyewall replacement dynamics is founded on axisymmetric balance dynamics reasoning with comparatively little quantitative testing. We use an illustrative example of a canonical eyewall replacement cycle to ascertain whether the radial contraction of the simulated outer eyewall is captured by the axisymmetric balance dynamics of convective rings. Our analysis reveals a significant weakness of the classical model and highlights the necessity of the boundary layer spinup mechanism (Smith et al. 2009; Montgomery and Smith 2014) to explain the phenomenon of eyewall replacement cycles in the presence of realistic heating and tangential momentum sources–sinks.

2. Methodology, models, and their integration

We revisit the Regional Atmospheric Modeling System (RAMS) integration studied by Terwey and Montgomery (2008), Terwey et al. (2013), Abarca and Montgomery (2013, 2014, hereafter AM14), and Montgomery et al. (2014). As shown in these studies, the simulation undergoes a canonical ERC. We adopt the methodology described in AM14 and apply it to the RAMS simulation

Corresponding author address: Sergio F. Abarca, Naval Postgraduate School, 589 Dyer Road, Root Hall, Room 254, Monterey, CA 93943.
E-mail: sergio.abarca.fuente@gmail.com

DOI: 10.1175/JAS-D-14-0151.1

Report Documentation Page

Form Approved
OMB No. 0704-0188

1. REPORT DATE	2. REPORT TYPE	3. DATES COVERED
JAN 2015		**00-00-2015 to 00-00-2015**

4. TITLE AND SUBTITLE	5a. CONTRACT NUMBER
Are Eyewall Replacement Cycles Governed Largely by Axisymmetric Balance Dynamics?	5b. GRANT NUMBER
	5c. PROGRAM ELEMENT NUMBER
6. AUTHOR(S)	5d. PROJECT NUMBER
	5e. TASK NUMBER
	5f. WORK UNIT NUMBER
7. PERFORMING ORGANIZATION NAME(S) AND ADDRESS(ES) **Naval Postgraduate School,Department of Meteorology,Monterey,CA,93943**	8. PERFORMING ORGANIZATION REPORT NUMBER
9. SPONSORING/MONITORING AGENCY NAME(S) AND ADDRESS(ES)	10. SPONSOR/MONITOR'S ACRONYM(S)
	11. SPONSOR/MONITOR'S REPORT NUMBER(S)

12. DISTRIBUTION/AVAILABILITY STATEMENT
Approved for public release; distribution unlimited

13. SUPPLEMENTARY NOTES

14. ABSTRACT

The authors question the widely held view that radial contraction of a secondary eyewall during an eyewall replacement cycle is well understood and governed largely by the classical theory of axisymmetric balance dynamics. The investigation is based on a comparison of the secondary circulation and derived tangential wind tendency between a full-physics simulation and the Sawyer???Eliassen balance model. The comparison is made at a time when the full-physics model exhibits radial contraction of the secondary eyewall during a canonical eyewall replacement cycle. It is shown that the Sawyer???Eliassen model is unable to capture the phenomenology of secondary eyewall radial contraction because it predicts a net spindown of the boundary layer tangential winds and does not represent the boundary layer spinup mechanism that has been articulated in recent work.

15. SUBJECT TERMS

16. SECURITY CLASSIFICATION OF:			17. LIMITATION OF ABSTRACT	18. NUMBER OF PAGES	19a. NAME OF RESPONSIBLE PERSON
a. REPORT	b. ABSTRACT	c. THIS PAGE			
unclassified	**unclassified**	**unclassified**	**Same as Report (SAR)**	**6**	

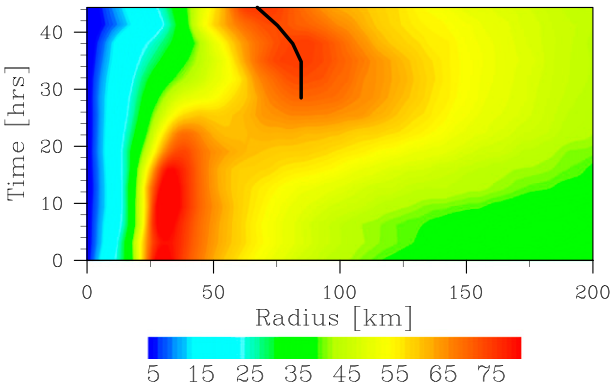

FIG. 1. Radius–time plot of the RAMS azimuthally averaged tangential velocity ($m\,s^{-1}$) at 787-m height. The black curve indicates the radius of maximum winds from hour 28 onward and highlights the radial contraction of the secondary eyewall.

at hour 36.[1] We follow the time convention of Terwey and Montgomery (2008) of renaming hour 156 as hour 0; unlike AM14, however, we use azimuthal averages of the RAMS data that have not been averaged in time.[2]

In a nutshell, the present methodology consists of using the RAMS output to characterize the mean vortex and its forcings in the Sawyer–Eliassen equation, and to compare the balanced secondary circulation and derived tangential wind tendency, against the corresponding fields from the full-physics model forecast. Details of the model integrations are found in AM14 (their section 2). The results presented here are not dependent on the precise choice of the time during the eyewall contraction and, for brevity, only one time is chosen to communicate the essential findings.

3. Results

The kinematics and dynamics of the modeled secondary eyewall formation have been analyzed in detail by Terwey and Montgomery (2008), Terwey et al. (2013), Abarca and Montgomery (2013), AM14, and Montgomery et al. (2014). Figure 1 shows a radius–time diagram of the azimuthally averaged tangential velocity at the model height of 787 m. This figure shows the evolution of the tangential wind field within the boundary layer[3] during the modeled ERC. At the height shown, the tangential wind maximum is initially centered at about 30-km radius and intensifies until about hour 15. At that time, the maximum tangential wind begins to weaken and to expand in radius (with the maximum located at roughly 42-km radius by hour 26). Prior to the weakening of the primary eyewall, the tangential winds outside the primary eyewall exhibit a progressive radial amplification that spans the mid- to lower troposphere. Such radial amplification extends to the boundary layer and can be seen in Fig. 1 (as exemplified by the $40\,m\,s^{-1}$ color shading).

The secondary wind maximum occurs in a relatively localized radial region, roughly centered at about 84-km radius (at the height shown here). The maximum occurs within the broad range of radii that experiences a radial expansion of the cyclonic tangential wind field. At the height shown, the secondary wind maximum represents the largest tangential winds of the storm from hour 26 onward, as the primary eyewall decays.

The secondary wind maximum contracts in radius, at an approximately constant rate of about $2\,km\,h^{-1}$ from hour 36 to hour 44, thereby completing the ERC. To assess to what extent balance dynamics captures the radial contraction of the secondary eyewall, we focus on hour 36 and neighboring times in the present analysis of this numerical simulation.

Figure 2 shows the azimuthally averaged kinematic and thermodynamical structure of the RAMS simulation, along with the corresponding averaged diabatic heating rate and the generalized tangential momentum sink at hour 36. These fields are used to characterize the mean vortex and its forcings, as required for the Sawyer–Eliassen balance inversion described in AM14. Figure 2a shows that, at hour 36, the largest tangential wind maximum occurs in the new single eyewall of the storm and is located within, but near the top of, the frictional boundary layer. At this time, the outer eyewall is contracting inward as part of the canonical ERC (Fig. 1). Figure 2b shows that the azimuthally averaged potential temperature field captures the broad warm-core structure of the storm, with the 360-K isotherm sloping upward from 9 to 13.5 km between the center of the storm and 150-km radius.

The mean diabatic heating rate (Fig. 2c) exhibits both a well-defined maximum associated with the new single eyewall of the storm and some relative maxima associated with convective activity radially inward and outward from the main eyewall. The generalized tangential momentum sink (Fig. 2d) exhibits its largest values in a shallow layer just above the surface and below the region of maximum tangential winds. Such a sink is attributable to surface friction that, by itself, acts to decelerate the tangential wind. The generalized tangential momentum forcing exhibits also sources and sinks above the boundary layer.

[1] The three pathways to characterize the vortex described in AM14 render results consistent with each other. Here, for brevity, we present only results of using the azimuthal-average setup, described in appendix B of AM14.

[2] Time average or lack of it does not change the main results or conclusions of this manuscript.

[3] As in previous studies, the boundary layer is defined dynamically as the shallow layer of strong inflow near the sea surface that arises largely because of the frictional disruption of gradient wind balance.

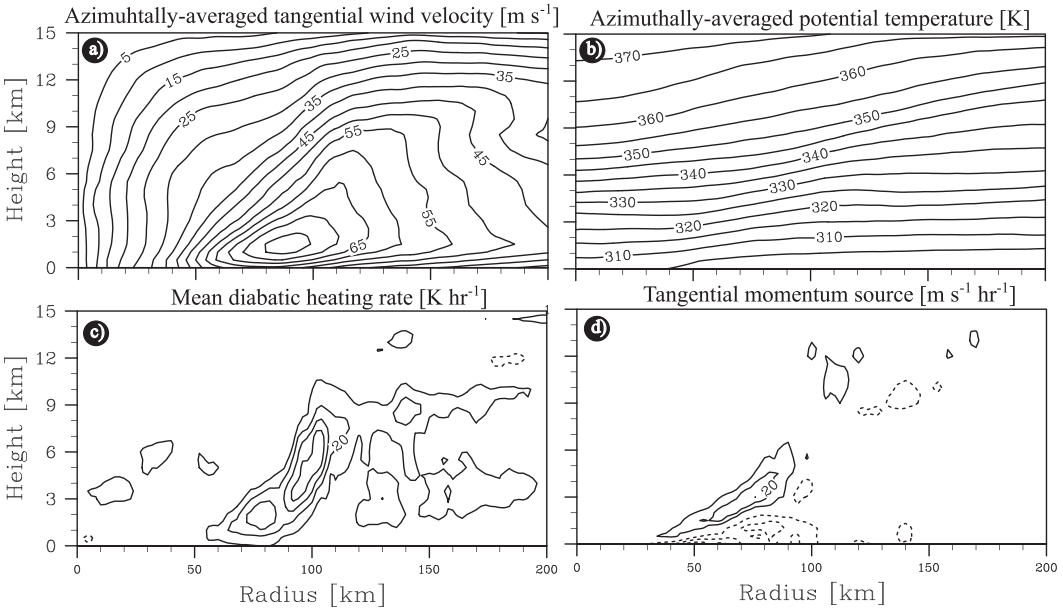

FIG. 2. Radius–height sections of the RAMS (a) azimuthally averaged tangential velocity, (b) azimuthally averaged potential temperature, (c) mean diabatic heating rate, and (d) tangential momentum source (see text for definitions of the last two quantities). The plots correspond to hour 36. Contours are shown every 5 units in (a),(b) and every 10 units in (c),(d). Solid lines represent positive values and dashed lines represent negative values.

These are located radially inward and outward from the main eyewall updraft and are associated with radial and vertical fluxes of eddy vertical vorticity and eddy tangential velocity (not shown separately), respectively.

Figure 3 compares the azimuthally averaged radial and vertical velocities and the azimuthally averaged tangential wind tendency of the RAMS integration at hour 36 with those resulting from the Sawyer–Eliassen balance inversion, calculated as described in AM14. The tendency of the tangential velocity field is computed according to the complete tangential momentum equation:

$$\frac{\partial \overline{v}}{\partial t} = -\overline{u}(\overline{\zeta} + f) - \overline{w}\frac{\partial \overline{v}}{\partial z} + F_{\lambda}\,. \qquad (1)$$

Here, as is customary, $\overline{u}$, $\overline{v}$, and $\overline{w}$ are the azimuthally averaged radial, tangential, and vertical wind velocities, respectively, t is time, $\overline{\zeta} = (1/r)[\partial(r\upsilon)/\partial r]$ is the azimuthally averaged relative vertical vorticity, f is the Coriolis parameter (evaluated at 15°N, as in the RAMS simulation), and F_{λ} is the generalized tangential momentum sink/source (computed as described in AM14). An overbar denotes azimuthal averages on constant height surfaces.

Figures 3a–d show that the Sawyer–Eliassen balance inversion captures the overall main features of the secondary circulation in the RAMS simulation. Specifically, Figs. 3a and 3b show that both RAMS and the Sawyer–Eliassen inversion exhibit inflow–outflow patterns typical of a mature hurricane, with inflow in the boundary layer and outflow in the upper troposphere and just above the boundary layer inflow. However, although the Sawyer–Eliassen inversion captures the general pattern of these broad features, it fails to capture the mid- and upper-level inflow exhibited by the RAMS integration (roughly centered at about 8.5-km height near the 200-km radius). In addition, the Sawyer–Eliassen inversion greatly underestimates the magnitude of boundary layer inflow. The largest value of the RAMS inflow exceeds 28 m s^{-1}, while the corresponding inflow in the Sawyer–Eliassen inversion never exceeds 16 m s^{-1}. Unlike the boundary layer inflow maximum, the magnitude of the outflow maximum in the upper-tropospheric outflow layer is captured reasonably well by the Sawyer–Eliassen inversion, with both integrations exhibiting outflow of about 25 m s^{-1} radially outward of 150 km. Figures 3c and 3d show also that the Sawyer–Eliassen inversion captures the general structure of the azimuthally averaged vertical motions exhibited by the RAMS integration but underestimates their maximum magnitude (by about 0.5 m s^{-1}).

Figure 3e shows the pattern of tangential wind tendency as predicted by RAMS. The pattern contains a clear signal of a contracting eyewall during the ERC, with positive tendencies radially inward from the eyewall location (see Figs. 2a and 2c), that spans the troposphere. The figure shows maxima in the tangential spinup rate with values of about 2.6 m s^{-1} h^{-1}. Outside the region of eyewall contraction and spinup, through the remaining domain, the tangential wind tendencies are negative.

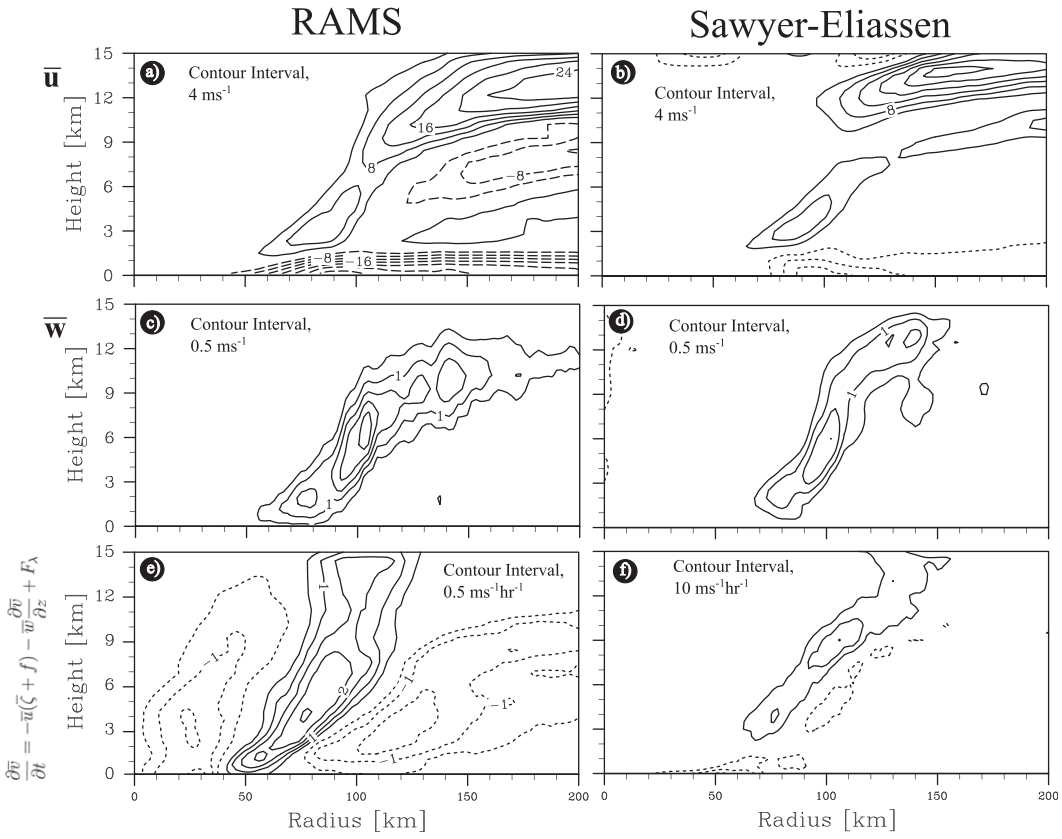

FIG. 3. Radius–height sections of the secondary circulations, and corresponding tangential wind tendencies, of (a),(c),(e) the RAMS integration and (b),(d),(f) the Sawyer–Eliassen integration. (a),(b) Radial velocity (contours every 4 m s^{-1}), (c),(d) vertical velocity (contours every 0.5 m s^{-1}), and (e),(f) tangential wind tendency (contours every 0.5 and 10 and m s^{-1} h^{-1}, respectively; see text for definitions of the tangential wind tendency). The RAMS data are azimuthally averaged and correspond to hour 36. Solid lines represent positive values and dashed lines represent negative values.

Figure 3f shows that, like the RAMS simulation, the Sawyer–Eliassen inversion exhibits spinup radially inward from the location of the outwardly sloping eyewall. However, unlike the RAMS simulation, the Sawyer–Eliassen inversion (including the frictional forcing of tangential velocity diagnosed from RAMS) exhibits a net spindown in the boundary layer. This creates a conundrum for the convective ring model: The predicted net spindown of the low-level tangential flow is not consistent with the predicted net spinup of the interior vortex by the lofting of low-level tangential momentum from the boundary layer.[4]

Higher up in the troposphere (around 9-km height), the Sawyer–Eliassen inversion substantially overestimates the magnitudes of the tangential wind tendency, with spinup reaching 30 m s^{-1} h^{-1} (at 104-km radius). These spinup values are an order of magnitude larger than those found in RAMS.

To shed light on the reasons for the poor performance of the Sawyer–Eliassen inversion, we present now the relative contributions of the mean radial vorticity flux and the mean vertical advection of tangential velocity.

Figure 4 shows the relative contributions to the mean tangential wind tendency from the mean radial vorticity flux and the mean vertical advection of mean tangential momentum for both RAMS and the Sawyer–Eliassen model. For the RAMS integration, Fig. 4a shows that the mean radial vorticity flux induces a positive tangential wind tendency throughout the boundary layer, with a maximum located between 70- and 86-km radius—that is, just inside of the tangential wind maxima (Fig. 2a). The maximum tangential wind tendency occurs radially inward of these radii (Fig. 3e), where the tangential

[4] These results hold true even when doubling or tripling the value of the generalized tangential momentum sink near the model surface. Such an exercise has been carried out following a reviewer's suggestion to account for any possible underestimation of the magnitude of the momentum sink at the lowest levels. Such underestimation could be possible given that the lowest model level explicitly represented in the RAMS integration is 148-m height (and not lower).

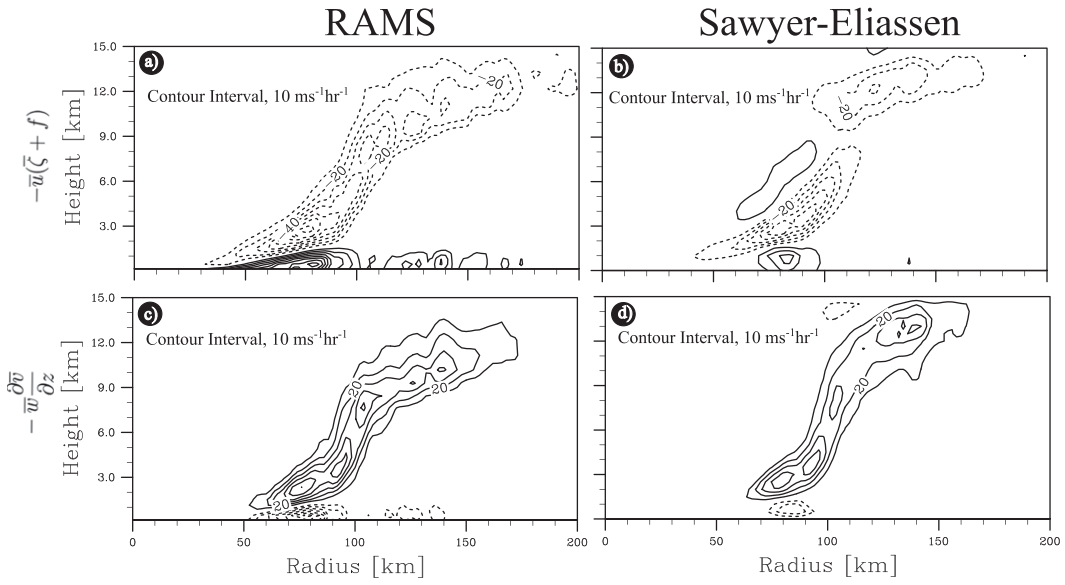

FIG. 4. Radius–height sections of (a),(b) mean absolute vorticity flux and (c),(d) mean vertical advection of mean tangential momentum for (a),(c) the RAMS and (b),(d) the Sawyer–Eliassen integrations. The RAMS panels correspond to hour 36. Contours are every $10\,\mathrm{m\,s^{-1}\,h^{-1}}$. Solid lines represent positive values and dashed ones represent negative values.

momentum sink (Fig. 2d) and the vertical advection (Fig. 4c) are smaller in magnitude. Figure 4a shows also that the mean radial vorticity flux induces only negative tendencies above the boundary layer, with the largest values located within the outwardly sloping eyewall (Figs. 2a and 3c), in a region that is dominated by the low-level outflow just above the strong inflow layer (Fig. 3a). Figure 4c shows that the mean vertical advection of mean tangential momentum has a negative tendency in the boundary layer in the region of the mean updraft (Fig. 3c) and a positive tendency within and above the contracting eyewall (Figs. 2a and 3c) in the rest of the troposphere.

Like the RAMS integration, Fig. 4b shows that the secondary circulation resulting from the Sawyer–Eliassen inversion yields a mean radial vorticity flux and a positive tangential wind tendency in the boundary layer with a maximum located around 84-km radius, radially inward of the tangential wind maxima (Fig. 2a). Unlike the RAMS integration, the mean radial vorticity flux deduced from the Sawyer–Eliassen inversion induces both negative and positive tendencies above the boundary layer.

Despite the qualitative similarity of the advective tendencies in the boundary layer between the two models, the mean radial vorticity flux is greatly underestimated by the Sawyer–Eliassen inversion, with a maximum positive tendency barely surpassing $30\,\mathrm{m\,s^{-1}\,h^{-1}}$ and the maximum negative tendency just reaching $-50\,\mathrm{m\,s^{-1}\,h^{-1}}$. When compared to the RAMS predictions, these balanced tendencies represent roughly a 60% and 30% underestimation, respectively.

Figure 4d shows that the mean vertical advection of mean tangential momentum in the Sawyer–Eliassen model induces a negative tendency in the boundary layer in the region of the mean updraft (Fig. 3c) and a positive tendency within and above the eyewall (Fig. 2a and 3c). This finding does resemble its RAMS counterpart (Fig. 4c). However, as in the case of the radial vorticity flux, the vertical advection of tangential momentum in the Sawyer–Eliassen model significantly underestimates the corresponding tendencies found in RAMS. Specifically, the largest negative tendency associated with the mean vertical advection in the boundary layer is underestimated by about 70%; the largest positive tendency associated with mean vertical advection above the boundary layer is underestimated by about 20%.

4. Summary and conclusions

The results of this investigation provide a quantitative basis for questioning the widely held view that eyewall replacement cycles in realistic hurricane vortices are now well understood and governed largely by the axisymmetric balance dynamics of convective rings. The results herein show that there are important quantitative differences in secondary circulations between the Sawyer–Eliassen and full-physics models and that such differences translate into striking differences in the tangential wind tendency and predicted evolution of the secondary eyewall.

In the full-physics model, the contraction of the eyewall is most pronounced in the boundary layer, where it occurs through the mean radial vorticity flux exceeding the direct spindown tendencies of mean tangential momentum by surface friction and mean vertical advection. This low-level radial vorticity flux has a component traceable to the axisymmetric balance dynamics of a convective ring driven by heat and tangential momentum forcing. However, the boundary layer spinup mechanism (as articulated in recent work comprising the nonlinear boundary layer flow and its coupling to the vortex interior) constitutes the dominant contribution to the radial vorticity flux, rendering a positive spinup tendency and hence contraction of the eyewall in the boundary layer. Above the boundary layer, the contracting eyewall occurs not through the horizontal flux of vertical vorticity but, rather, primarily through the mean vertical advection of tangential momentum out of the boundary layer.

In striking contrast to the full-physics model, the balance model of a convective ring yields a net spindown of the boundary layer and thus is unable to represent the contraction of the eyewall as it occurs in the full-physics model. Although the balance model does render a positive tangential velocity tendency radially inward of the primary eyewall, this positive tendency occurs only above the boundary layer and occurs mostly because of the upward vertical advection of tangential momentum from the eyewall. The predicted net spindown of the low-level tangential flow, in juxtaposition with the net spinup of the interior vortex by the lofting of tangential momentum, creates a conundrum for the convective ring model. The boundary layer spinup mechanism is needed to resolve the conundrum and render a self-consistent consistent mechanism of eyewall contraction.

Acknowledgments. This work was supported in part by National Science Foundation Awards AGS 0733380 and IAA-1313948. Sergio F. Abarca gratefully acknowledges the support from the National Research Council (NRC) through its Research Associateship Program, and the host institution, the Naval Postgraduate School (NPS) in Monterey, California. The authors thank Professor Roger Smith for reading a draft of the manuscript and offering suggestions that helped clarify the presentation.

REFERENCES

Abarca, S. F., and M. T. Montgomery, 2013: Essential dynamics of secondary eyewall formation. *J. Atmos. Sci.,* **70,** 3216–3230, doi:10.1175/JAS-D-12-0318.1.

——, and ——, 2014: Departures from axisymmetric balance dynamics during secondary eyewall formation. *J. Atmos. Sci.,* **71,** 3723–3738, doi:10.1175/JAS-D-14-0018.1.

Kepert, J. D., 2010: Tropical cyclone structure and dynamics. *Global Perspectives on Tropical Cyclones: From Science to Mitigation,* J. C. L. Chan and J. D. Kepert, Eds., World Scientific Series on Asia-Pacific Weather and Climate, Vol. 4, World Scientific, 3–54.

——, 2013: How does the boundary layer contribute to eyewall replacement cycles in axisymmetric tropical cyclones? *J. Atmos. Sci.,* **70,** 2808–2830, doi:10.1175/JAS-D-13-046.1.

Montgomery, M. T., and R. K. Smith, 2014: Paradigms for tropical-cyclone intensification. *Aust. Meteor. Oceanogr. J.,* **64,** 1–30.

——, S. F. Abarca, R. K. Smith, C. C. Wu, and Y. H. Huang, 2014: Comments on ''How does the boundary layer contribute to eyewall replacement cycles in axisymmetric tropical cyclones?'' *J. Atmos. Sci.,* **71,** 4682–4691, doi:10.1175/JAS-D-13-0286.1.

Rozoff, C. M., W. H. Schubert, and J. P. Kossin, 2008: Some dynamical aspects of hurricane eyewall replacement cycles. *Quart. J. Roy. Meteor. Soc.,* **134,** 583–593, doi:10.1002/qj.237.

Shapiro, L. J., and H. E. Willoughby, 1982: The response of balanced hurricanes to local sources of heat and momentum. *J. Atmos. Sci.,* **39,** 378–394, doi:10.1175/1520-0469(1982)039<0378:TROBHT>2.0.CO;2.

Smith, R. K., M. T. Montgomery, and N. V. Sang, 2009: Tropical cyclone spin-up revisited. *Quart. J. Roy. Meteor. Soc.,* **135,** 1321–1335, doi:10.1002/qj.428.

Terwey, W. D., and M. T. Montgomery, 2008: Secondary eyewall formation in two idealized, full-physics modeled hurricanes. *J. Geophys. Res.,* **113,** D12112, doi:10.1029/2007JD008897.

——, S. F. Abarca, and M. T. Montgomery, 2013: Comments on ''Convectively generated potential vorticity in rainbands and formation of the secondary eyewall in Hurricane Rita of 2005.'' *J. Atmos. Sci.,* **70,** 984–988, doi:10.1175/JAS-D-12-030.1.

Willoughby, H. E., 1988: The dynamics of the tropical cyclone core. *Aust. Meteor. Mag.,* **36,** 183–191.

——, 1990: Gradient wind balance in tropical cyclones. *J. Atmos. Sci.,* **47,** 265–274.

——, J. A. Clos, and M. G. Shoreibah, 1982: Concentric eye walls, secondary wind maxima, and the evolution of the hurricane vortex. *J. Atmos. Sci.,* **39,** 395–411, doi:10.1175/1520-0469(1982)039<0395:CEWSWM>2.0.CO;2.

Zhu, Z., and P. Zhu, 2014: The role of outer rainband convection in governing the eyewall replacement cycle in numerical simulations of tropical cyclones. *J. Geophys. Res. Atmos.,* **119,** 8049–8072, doi:10.1002/2014JD021899.